

See discussions, stats, and author profiles for this publication at: <https://www.researchgate.net/publication/277086550>

Size-Based Separation of Particles and Cells Utilizing Viscoelastic Effects in Straight Microchannels

Article in *Analytical Chemistry* · May 2015

Impact Factor: 5.64 · DOI: 10.1021/acs.analchem.5b00516 · Source: PubMed

CITATIONS

3

READS

83

6 authors, including:



Chao Liu

Chinese Academy of Sciences

11 PUBLICATIONS 145 CITATIONS

SEE PROFILE



Xiaodong Chen

Chinese Academy of Sciences

37 PUBLICATIONS 107 CITATIONS

SEE PROFILE



Guoqing Hu

Chinese Academy of Sciences

52 PUBLICATIONS 686 CITATIONS

SEE PROFILE

Size-based Separation of Particles and Cells Utilizing Viscoelastic Effects in Straight Microchannels

Chao Liu, Chundong Xue, Xiaodong Chen, Lei Shan, Yu Tian, and Guoqing Hu

Anal. Chem., **Just Accepted Manuscript** • Publication Date (Web): 19 May 2015

Downloaded from <http://pubs.acs.org> on May 19, 2015

Just Accepted

“Just Accepted” manuscripts have been peer-reviewed and accepted for publication. They are posted online prior to technical editing, formatting for publication and author proofing. The American Chemical Society provides “Just Accepted” as a free service to the research community to expedite the dissemination of scientific material as soon as possible after acceptance. “Just Accepted” manuscripts appear in full in PDF format accompanied by an HTML abstract. “Just Accepted” manuscripts have been fully peer reviewed, but should not be considered the official version of record. They are accessible to all readers and citable by the Digital Object Identifier (DOI®). “Just Accepted” is an optional service offered to authors. Therefore, the “Just Accepted” Web site may not include all articles that will be published in the journal. After a manuscript is technically edited and formatted, it will be removed from the “Just Accepted” Web site and published as an ASAP article. Note that technical editing may introduce minor changes to the manuscript text and/or graphics which could affect content, and all legal disclaimers and ethical guidelines that apply to the journal pertain. ACS cannot be held responsible for errors or consequences arising from the use of information contained in these “Just Accepted” manuscripts.



Size-based Separation of Particles and Cells Utilizing Viscoelastic Effects in Straight Microchannels

Chao Liu,[†] Chundong Xue,[†] Xiaodong Chen,[†] Lei Shan,[‡] Yu Tian,[‡] and Guoqing Hu^{*,†}

[†]State Key Laboratory of Nonlinear Mechanics, Beijing Key Laboratory of Engineered Construction and Mechanobiology, Institute of Mechanics, Chinese Academy of Sciences, Beijing 100190, China.

[‡]State Key Laboratory of Tribology, Tsinghua University, Beijing 100084, China.

*To whom correspondence should be addressed. Email: guoqing.hu@imech.ac.cn (Dr. Hu). Tel: 86-10-82544298; Fax: 86-10-82543977.

ABSTRACT: Viscoelasticity-induced particle migration has recently received increasing attention due to its ability to obtain high-quality focusing over a wide range of flow rates. However, its application is limited to low throughput regime since the particles can defocus as flow rate increases. Using an engineered carrier medium with constant and low viscosity and strong elasticity, the sample flow rates are improved to be one order of magnitude higher than those in existing studies. Utilizing differential focusing of particles of different sizes, here we present sheathless particle/cell separation in simple straight microchannels that possess excellent parallelizability for further throughput enhancement. The present method can be implemented over a wide range of particle/cell sizes and flow rates. We successfully separate small particles from larger particles, MCF-7 cells from red blood cells (RBCs), and *Escherichia coli* (*E. coli*) bacteria from RBCs in different straight microchannels. The proposed method could broaden the applications of viscoelastic microfluidic devices to particle/cell separation due to the enhanced sample throughput and simple channel design.

Continuous manipulation and separation of particles and cells is important for a wide range of applications in biology,^{1,2} medicine,^{2,3} and industry.^{4,6} Microfluidic systems have been proven to be promising tools for particle/cell manipulation with higher sensitivity and accuracy than their macroscale counterparts. The last decade has seen extensive development of microfluidic approaches for particle/cell manipulation that resort to immunocapture,⁷ externally applied physical fields,⁸⁻¹⁸ microfiltration,^{19,20} gravitational sedimentation,²¹ or deterministic lateral migration.^{22,23} More recently, cross-streamline migration induced by the hydrodynamic effects of carrier media, such as inertia^{24,25} and viscoelasticity,^{26,27} has shown its promise for effective particle/cell manipulation without need of labeling and external force fields. Particles and cells can be separated based on the size-dependent nature of hydrodynamic forces. Briefly, the inertial lift scales as $F_i \propto a^4$ and the viscoelastic lift scales as $F_e \propto a^3$, where a is the particle diameter. There are several cell types of biological and clinical interest with separable size ranges: epithelial tumor cells (15–25 μm in diameter), blood cells (erythrocytes are 6–8 μm biconcave disks and peripheral blood lymphocytes are 7–10 μm in diameter), and bacteria (1–3 μm). Inertial migration in Newtonian fluids has been intensively studied and implemented in high-throughput label-free separation devices for cell separation.²⁸⁻³⁴

Recently, particle migration induced by viscoelasticity has begun to attract increasing attention due to its simple focusing pattern and potential for achieving efficient focusing over a wide range of flow rates.^{35,36} In a viscoelastic medium, elasticity coupled with non-negligible inertia will drive particles towards the channel centerline, which is more desirable for focusing and further manipulation compared to the pure inertial focusing. Moreover, inertial focusing pattern becomes more complex at higher Reynolds number Re , often resulting in unfavorable multiple lateral equilibrium positions.³⁷ Considering the condition of $a/D_h > 0.07$ for successful inertial focusing of particles,³⁸ the channel

cross-section has to be scaled down with decreasing particle sizes [D_h , the hydraulic diameter, is defined as $2WH/(W+H)$, where W and H are the channel width and height, respectively]. For inertial manipulation of sub-micron particles in a relatively small channel, extremely high pressure is required to push moderate Re flows, since the flow resistance is inversely proportional to H^3W .³⁹ In contrast, the presence of elastic stresses can still induce deterministic lateral migration of particles even at very low flow rates.

Microfluidic devices utilizing viscoelasticity have been developed for focusing and separation of particles and cells. The most commonly used viscoelastic media are aqueous solution of poly(ethylene oxide) (PEO) and poly(vinylpyrrolidone) (PVP) that are biocompatible synthetic polymers. By properly balancing the inertial and elastic forces, Yang *et al.* obtained 3D focusing along the centerline of a square microchannel.⁴⁰ Kim *et al.* focused sub-micron DNA molecules at the channel centerline by taking advantage of the wall repulsion arising from DNA flexibility.⁴¹ There are two approaches to achieve viscoelastic separation, either by employing sheath flow (kinetic separation) or by engineering channel geometry (equilibrium separation). Nam *et al.* successfully separated platelets from diluted whole blood with high efficiency of 99% using a sheath flow microdevice where RBCs were focused along the centerline whereas platelets remained near the side walls.⁴² Lee *et al.* separated 10 μm and 1.5 μm particles in a single spiral microchannel by introducing a secondary flow. However, separation based on sheath flow often suffers from the reduced sample throughput. Curved channel design also faces the challenge of high pressure drop over the long channel, especially for highly viscous polymer solutions.

Viscoelastic focusing and separation using PEO or PVP normally work at 1-2 orders of magnitude slower flow speed than their inertial counterparts in the similar channel dimension, since the particle defocusing occurs as Re increases beyond order of unity. One explanation is that the shear-gradient lift arising from fluid inertia tends to drive

particles away from the channel centerline, indicating that enhancing medium elasticity to balance the shear gradient lift is an effective strategy for improving throughput. Recently, Kang *et al.* used a high relaxation time medium (5 ppm λ -DNA solution, $\lambda = 0.14$ s) to obtain high-quality particle focusing over a wide range of flow rates (0.005–2 ml/h).³⁵ Another explanation for the particle defocusing is the destabilization of elastically dominated flow at high Weissenberg number Wi .⁴³ The flow will be stabilized when inertia and elasticity simultaneously dominate,^{44,45} indicating a strategy of reducing the relative importance of medium elasticity. Lim *et al.* also reported particle focusing at extremely high flow rates (1200 ml/h, $Re = 4630$, $Wi = 566$) using a medium with low relaxation time [0.1 w/v % hyaluronic acid (HA) solution, $\lambda = 8.7 \times 10^{-4}$ s].³⁶ The inconsistency between these two explanations may imply an inconclusive understanding of viscoelastic migration. Though having revolutionized viscoelastic focusing, these methods are limited in applications by the high cost of DNA and HA solutions (Table S1).

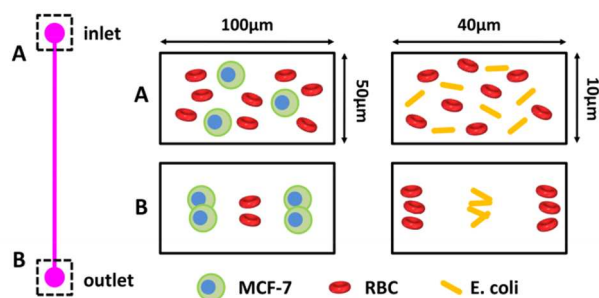


Figure 1. The schematic of straight microchannels with rectangular cross-section illustrating the cell separation (not to scale). The separation is based on the size difference between the sorted cell types and works well in a wide range of spatial scales. At the outlet, the large MCF-7 cells/RBCs are focused near the side walls whereas the small RBCs/*E. coli* bacteria are focused along the channel centerline.

Here we demonstrate label-free, sheathless, and inexpensive separations of particles and cells by size in straight rectangular microchannels. Interestingly, particles with blockage ratio $\kappa = 0.3$ ($\kappa = a/H$) will migrate towards the lateral positions near the two side walls, which is different from the traditional focusing pattern of one focusing position at the channel centerline. Exploiting this unexpected mechanism, we realize complete separation of particles with a wide range of length scales—the large components are focused near the side walls whereas the small components are focused along the centerline. High-quality separation of two types of binary mixtures of biparticles—MCF-7 cells/RBCs and *E. coli* bacteria/RBCs—can also be easily achieved due to their difference in size (Figure 1). In addition, the operational flow rates can reach one order of magnitude higher than those in existing studies by engineering the rheological properties of the carrier medium. The sample throughput can be further improved due to the excellent parallelizability of this extremely simple design using straight microchannels.

DESIGN PRINCIPLES

The fluid viscoelasticity can be characterized by Weissenberg number Wi ($Wi = \lambda \dot{\gamma}$, where $\dot{\gamma}$ is the strain rate) that is the

ratio of elastic force to viscous force. In this work, the characteristic strain rate is defined as $2Q_v/HW^2$ that is the ratio of the average flow velocity $U_a = Q_v/HW$ to the half channel width $W/2$. The Reynolds number Re ($Re = \rho U_a W/\eta$, where η is the viscosity) is the relative ratio of inertial force to viscous force. In a viscoelastic Poiseuille flow, suspended particles will laterally migrate towards specific equilibrium positions due to the nonuniform normal stress differences, i.e., the first (N_1) and the second (N_2) normal stress differences. The effect of N_2 is generally neglected due to its small magnitude compared to N_1 for most polymer solutions.⁴⁶ The elastic lift F_e on a particle arises from the imbalance of N_1 over the particle, and can be expressed as:²⁷

$$F_e = C_e a^3 \nabla N_1 \quad (1)$$

where C_e is the nondimensional coefficient. N_1 is scaled as $N_1 \propto \dot{\gamma}^2$. The strain rate $\dot{\gamma}$ is defined as $(2\mathbf{D}:\mathbf{D})^{1/2}$, where \mathbf{D} is the deformation rate tensor and is expressed as $\mathbf{D} = \nabla \mathbf{u}/2 + (\nabla \mathbf{u})^T/2$. For a fully developed flow in straight channels, $\dot{\gamma}$ is expressed as $\dot{\gamma} = [(\partial u/\partial y)^2 + (\partial u/\partial z)^2]^{1/2}$. In a pure elastic flow ($Wi > 0$, $Re \sim 0$), particles will migrate towards the centerline and four corners where $\dot{\gamma}$ has minimum (Figure 2a).

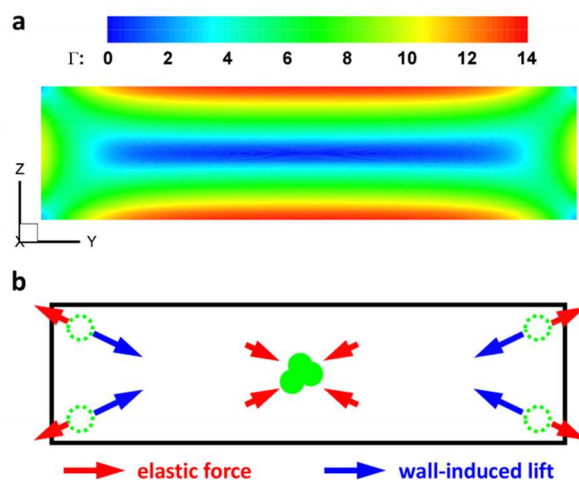


Figure 2. (a) The distribution of the nondimensional strain rate Γ in a microchannel with $AR = 4$, where the velocity and length scale were normalized by the average velocity U_a and the half channel width $W/2$, respectively. When the elasticity dominates, particles will be focused at the positions where Γ has minimum, i.e., the channel centerline and four corners. (b) In a viscoelastic flow with non-negligible inertia, particles will be only focused at the channel centerline since the wall-induced lift pushes the particles away from the corners.

The inertial lift often involves in the particle migration in viscoelastic media. It consists of two counteracting components: the shear-gradient lift that is directed towards the channel wall and the wall-induced lift that is directed towards the channel centerline. The wall-induced lift is about one order

of magnitude higher than the shear-gradient lift,^{19,20,44} and therefore the inertial lift has different effects on particle migration depending on flow conditions. In a flow with non-negligible inertia [$0 < Re < O(1)$], particles are only focused along the channel centerline due to synergetic combination of fluid elasticity and the wall-induced lift (Figure 2b). As Re increases [$Re \geq O(1)$], the shear-gradient lift becomes important and drives particles away from the channel centerline, resulting in particle defocusing.

EXPERIMENTAL SECTION

Sample Preparation. The PEO solution was prepared by adding PEO ($M_w = 4 \times 10^6$ g/mol, Sigma-Aldrich, USA) powder to 22 wt % glycerin (Sigma-Aldrich, USA) aqueous solution to match the density of the polystyrene (PS) particles (1.05×10^3 kg/m³). The PVP solution was prepared by dissolving PVP ($M_w = 3.6 \times 10^5$ g/mol, Sigma-Aldrich, USA) powder in deionized water. For the experiments in $H = 10$ μm channels, the suspensions of 1 μm and 3 μm PS particles (1 wt %, Phosphorex Inc., USA) were diluted in these experimental solutions to 0.005% and 0.01% volume fraction, respectively. For the experiments in $H = 50$ μm channels, the suspensions of 5 μm and 15 μm PS particles (1 wt %, Phosphorex Inc., USA) were diluted in these experimental solutions to 0.01% and 0.03% volume fraction, respectively. To prevent particle aggregation, surfactant Tween 20 (Sigma-Aldrich, USA) was added into the suspensions at 0.1 w/v %.

For cell experiments, the PEO solution was prepared by adding PEO ($M_w = 4 \times 10^6$ g/mol, Sigma-Aldrich, St. Louis, MO) powder to 1 \times phosphate buffered saline (PBS). Human blood sample was collected by a finger-pricking device (ACCU-CHEK Softclix, FP001, Roche, Switzerland) and stored at 4 $^\circ\text{C}$. Before use, the blood sample was diluted 40 times (1% hematocrit) with 1 \times PBS. MCF-7 cells (average diameter around 18 μm) were cultured in high-glucose Dulbecco's modified Eagle's medium (DMEM) containing 10% fetal bovine serum and 1% penicillin/streptomycin in a 5% CO₂, 37 $^\circ\text{C}$ incubator (Thermo Scientific, USA). *E. coli* bacteria were cultured in LB Broth (Sigma-Aldrich, USA) on a shaker at 37 $^\circ\text{C}$ for 12 h.

Fluid Rheology Measurements. The rheological properties were measured by a rheometer (Physica MCR301, Anton Paar GmbH, Germany) with cone-plate geometry (50 mm, 0.017 rad) at 25 $^\circ\text{C}$ (Figure 3). The steady shear viscosities were measured at the shear rates of 1-3000 s^{-1} (Figure 3a). The PVP solution has a zero-shear viscosity of 2.8×10^{-2} Pa.s and remains constant up to a shear rate of 1000 s^{-1} . Since the viscosity decreases less than 10% at the maximum experimental flow rate of 1.5 ml/h ($\dot{\gamma} = 1670$ s^{-1}) compared to the zero-shear viscosity, we neglect the influence of shear thinning behavior on particle migration. In contrast, the newly prepared 0.2 wt % PEO solution is shear thinning over the entire range of measured shear rates. Another PEO solution was denaturized by being stored at room temperature without direct exposure in sunlight for 3 months. Possessing a visibly decreasing viscosity at very low shear rates of 1-30 s^{-1} ,

the denaturized PEO solution has low viscosity of about 4×10^{-3} Pa.s at the shear rates of 30-3000 s^{-1} (Figure 3a).

Elastic moduli G^* of these solutions were measured in small-amplitude (1% amplitude) oscillatory test (Figure 3b). Figure 3b inset shows that the PVP solution have paradigmatic terminal behavior— $G^* \propto \omega^2$ and $G'' \propto \omega$ in a wide range of frequencies, where G'' is the viscous modulus. The relaxation time is estimated as 2.2×10^{-3} s by the intersection of the G^* and G'' curves.^{47,48} The relaxation time for the newly prepared PEO solution is estimated as 4.4×10^{-2} s by the empirical formula based on capillary breakup extension rheometry (CaBER) measurement: $\lambda = 18\lambda_z (c/c^*)^{0.65}$,⁴⁹

where λ_z is the Zimm relaxation time (1.1×10^{-3} s⁵⁰) and c^* the overlapping concentration (547 ppm⁵¹). Since $Wi \propto \lambda$, the newly prepared PEO solution will show stronger elasticity than the PVP solution in a given flow condition. In addition to the relaxation time, elastic modulus can also well characterize the fluid elasticity. Figure 3 shows that the denaturized PEO solution has almost the identical elastic modulus with the newly prepared one, allowing us to consider a negligible loss of elasticity.

Microchannel Design and Fabrication. We used straight microchannels with two different heights for experiments depending on the sizes of particles or cells. Microchannels that were 10 μm high and 30 mm long were used for PS particles with diameters of 1 μm and 3 μm ($\kappa = 0.1$ and 0.3, respectively) and for *E. coli* bacteria and RBCs. Microchannels that were 50 μm high and 50 mm long were used for PS particles with diameters of 5 μm and 15 μm ($\kappa = 0.1$ and 0.3, respectively) and for MCF-7 cells and RBCs. All the microchannels had one inlet and one outlet.

The microchannels were fabricated using the standard soft-lithography techniques with SU8-2050 master mold on a silicon substrate. The degassed poly(dimethylsiloxane) (PDMS) was cast over the mold and then was baked in an oven at 80 $^\circ\text{C}$ for 3 hr. The PDMS slab was punched through at the inlet and outlet to make ports and then plastic tubes were inserted through these ports with glue at the tube ends. The PDMS slab was then treated with oxygen plasma and bonded to a glass substrate (25 mm \times 75 mm). Finally the assembled device was placed into an oven at 70 $^\circ\text{C}$ for 30 min to enhance bonding.

Experimental Procedures and Image Analysis. Experimental liquid was injected into the microchannels using a syringe pump (Pump 11 Elite, Harvard Apparatus, USA). The flow rate was precisely adjusted by tuning the parameters of the pump. The chip containing the microchannel was mounted onto the stage of an inverted microscope (Eclipse Ti, Nikon, Japan). The dynamics of particles and cells were observed in a top view at the outlet, and the images and movies were recorded with a high-speed camera (Phantom v7.3, Vision Research Inc., USA) and Phantom Camera

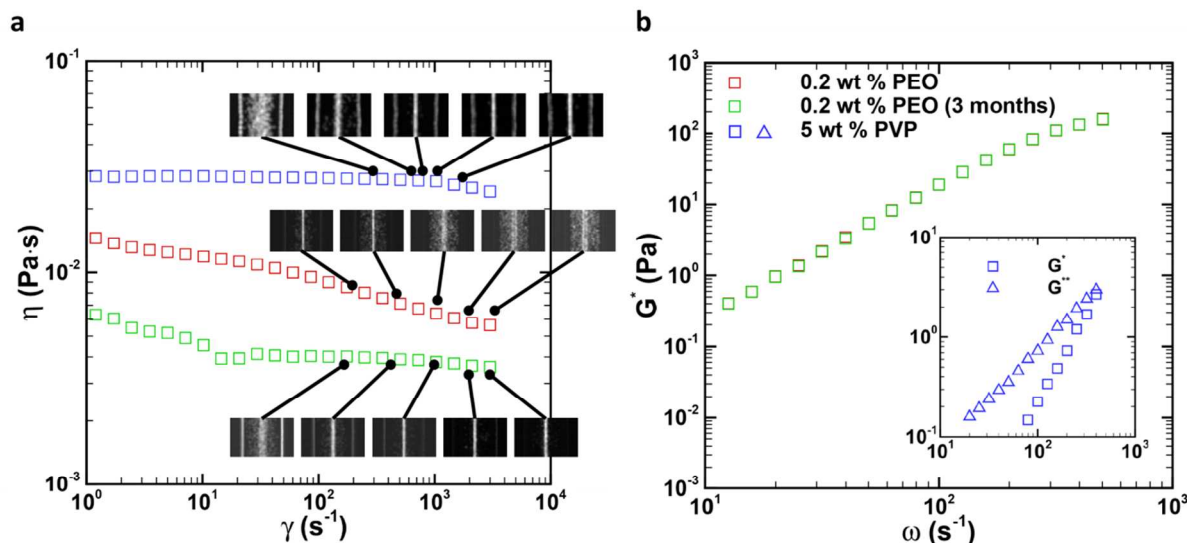


Figure 3. The shear dependence of the viscosities (a) and the frequency dependence of the viscoelastic moduli (b) of the investigated viscoelastic liquids. (a) The 5 wt % PVP solution and the denatured 0.2 wt % PEO solution have constant viscosities over the range of experimental shear rates, whereas the newly prepared 0.2 wt % PEO solution shows shear thinning behavior over the entire range of measured shear rates. The stacked images show the focusing patterns of 5 μm particles in microchannels with $H = 50 \mu\text{m}$ and $AR = 2$ using these three types of media and suggest that shear thinning has a good correlation with the particle defocusing with increasing flow rate. (b) The measurement of elastic modulus G^* shows that the denatured PEO solution has almost the same elasticity with the newly prepared one. The insert shows the measurement of the elastic modulus G^* and the viscous modulus G'' for the PVP solution.

Control software. The exposure time was reduced with increasing flow rates to prevent the fuzzy boundaries. The images were processed with the ImageJ software package (NIH): the time-series images (1000-2000 images) were stacked using z-projection with the 'standard deviation' option. The particle distributions were determined by conducting automatic particle analysis for 2000-4000 images (≥ 1000 particles) and the cell distributions were manually analyzed for 500-1000 images (≥ 10000 cells). Here, the purity is defined as the ratio of the targeted to the total cells, the enrichment factors is obtained by dividing the purities at the preferred outlet with the initial purities at the inlet, and the separation efficiency of a certain cell type is defined as its percentage at the preferred outlet.

RESULTS AND DISCUSSION

Engineering the rheological properties. The focusing behaviors of particles in a viscoelastic medium depend on the rheological properties, such as viscosity, shear dependence of viscosity, and elasticity. Three types of viscoelastic media (the newly prepared and denatured 0.2 wt % PEO, and 5 wt % PVP aqueous solutions) were used to investigate the particle focusing behavior. The particle focusing worsening with increasing flow rate is the major limiting factor of the throughput. Using a highly elastic fluid with constant and low viscosity can overcome this difficulty. Figure 3a shows the focusing patterns of 5 μm particles in microchannels with $H = 50 \mu\text{m}$ and $AR = 2$ using these three types of media, suggesting that shear thinning has a good correlation with the particle defocusing. In the newly prepared 0.2 wt % PEO solution, the particles along the centerline became defocused even at the lowest experimental flow rate of 0.2 ml/h ($Re = 0.14$, $\dot{\gamma} = 2.2 \times 10^2 \text{ s}^{-1}$). In the 5 wt % PVP and the denatured 0.2 wt % PEO solutions that have constant viscosities over the entire range of experimental flow rates, the focusing along the

centerline remained tight over a wide range of flow rates up to 1.5 ml/h ($Re = 0.3$, $\dot{\gamma} = 1.7 \times 10^3 \text{ s}^{-1}$) and 3.0 ml/h ($Re = 4.2$, $\dot{\gamma} = 3.3 \times 10^3 \text{ s}^{-1}$), respectively. The correlation between the particle defocusing and shear thinning is consistent with existing experimental and numerical observations showing that the shear thinning effect always drive the particle closer to the wall in viscoelastic fluids.^{47,52-54}

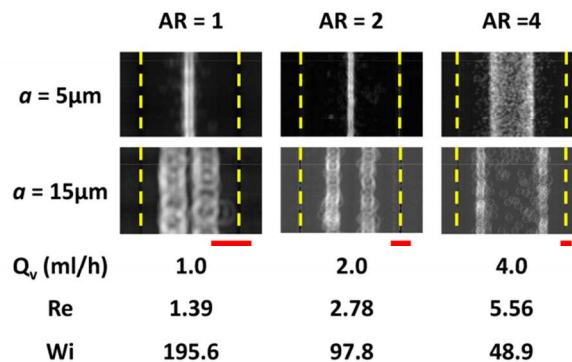


Figure 4. The size-dependent differential focusing behaviors of 15 μm and 5 μm particles in microchannels with $H = 50 \mu\text{m}$ are shown at the flow rates of 1.0, 2.0 and 4.0 ml/h for $AR = 1, 2$ and 4, respectively. The deviation from the centerline of the 15 μm particles ($\kappa = 0.3$) occurred for all the investigated AR . The carrier medium was the denatured 0.2 wt % PEO solution. Scale bars, 20 μm .

Fluids with high viscosities are also undesirable for particle manipulation, since throughput is limited by high pressure drop and multiple focusing pattern will exist over a wide range of flow rates due to low Re . In the 5 wt % PVP solution with high viscosity of $2.8 \times 10^{-2} \text{ Pa}\cdot\text{s}$, particles appeared at the channel corners even at 1.5 ml/h due to the low Re ($Re = 0.3$).

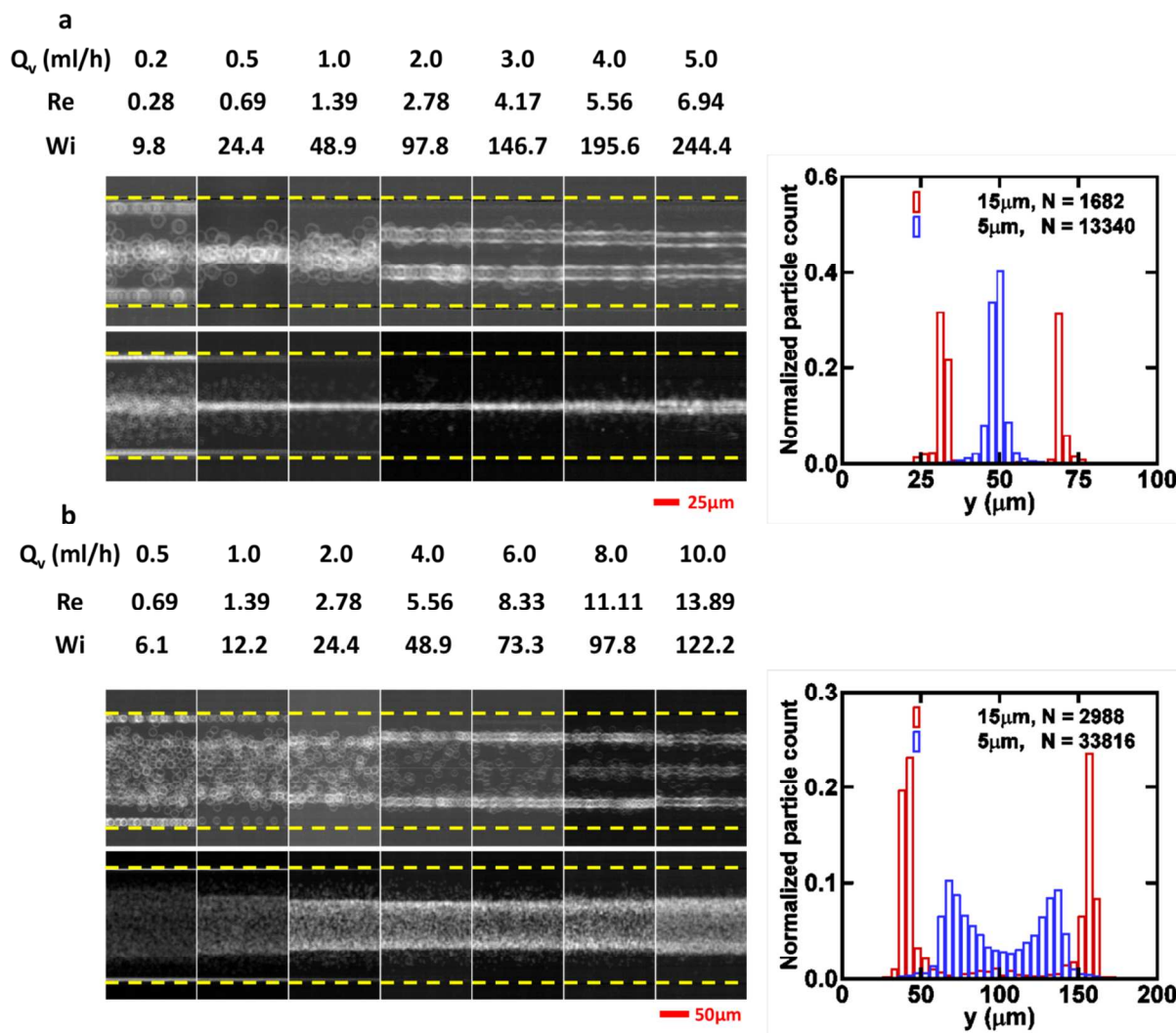


Figure 5. The distributions of 15 μm and 5 μm particles in $H = 50 \mu\text{m}$ microchannels with $AR = 2$ (a) and $AR = 4$ (b) using the denaturated 0.2 wt % PEO solutions suggest the remarkable size-dependent differential focusing. Stacked images are shown at a wide range of flow rates (0.2-5.0 ml/h for $AR = 2$ and 0.5-10.0 ml/h for $AR = 4$). Normalized particle count plots are shown at 3.0 ml/h and 6.0 ml/h for $AR = 2$ and $AR = 4$, respectively.

On the other hand, longer relaxation time is required for a medium with low viscosity to balance the enhanced shear-gradient lift, which can result in particle defocusing at higher flow rates. Longer λ can be achieved either by using a polymer with high M_w or by increasing polymer concentration c . To achieve sufficient elasticity, most existing studies on particle/cell separation use solutions of high-molecular-weight PEO [$M_w \sim O(10^6)$ g/mol] with optimized $c \geq 0.05$ wt %.^{40,42,55} However, their operational flow rates were limited to $O(0.1)$ ml/h due to the shear thinning effects, which is similar to the case of the newly prepared 0.2 wt % PEO. We find that the denaturated 0.2 wt % PEO has almost the identical elastic modulus with its newly prepared counterpart, but has constant and low viscosity. Using the denaturated PEO solution, we can overcome the aforementioned difficulties and obtain high-quality separation at one order of magnitude higher flow rates than previous studies. All following results were obtained by using the denaturated 0.2 wt % PEO solution unless stated otherwise.

Differential focusing and particle/cell separation. A particle with large blockage ratio tend to migrate more closely

towards the wall due to the enhanced compressive normal stress at the near-center side of the particle.^{54,56} Figure 4 shows that 15 μm particles ($\kappa = 0.3$) in the microchannels with $H = 50 \mu\text{m}$ were focused at the both sides of the centerline at optimized flow rates for all the investigated aspect ratios ($AR = 1, 2$ and 4). In contrast to the 15 μm particles, 5 μm particles ($\kappa = 0.1$) were focused along the centerline as observed in previous works.^{27,35,36,40,42,48,57} A large particle tends to migrate towards the wall when it displaces from the channel center. The major portion of fluid chooses to flow through the larger gap between the particle and the channel wall.⁵⁸ Therefore, the shear rates around a particle can be intensified, resulting in enhanced compressive normal stress at the near-center side of the particle.⁵⁴ As a consequence, large particles will be driven towards the wall. The off-center focusing has only been reported by numerical studies ($\kappa \geq 0.25$) and macroscale experiments ($\kappa = 0.6$).^{54,56} Most existing studies manipulate particles or cells with κ around 0.1 in square microchannels,^{27,35,36,42,48,57,59-61} and thus this off-center focusing was not discovered in these experiments. This off-center focusing is quite different from that in inertial flow

of Newtonian fluids. Particles suspended in a Newtonian fluid are focused at the centers of the long channel walls in rectangular microchannels^{24,62} because the particle migration is dominated only by the fluid inertia and the lift direction is independent of blockage ratio. Therefore, the difference in focusing nature leads to different separation strategy in straight channels — equilibrium separation in viscoelastic fluids and kinetic separation in Newtonian fluids.

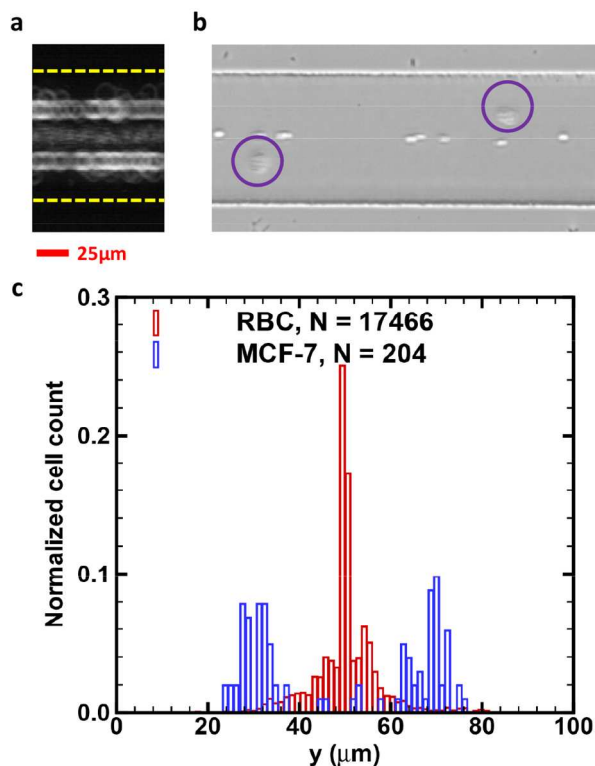


Figure 6. (a) The separation of the binary mixture of 15 μm and 5 μm particles is shown at the optimized flow rate of 3.0 ml/h ($Re = 4.17$ and $Wi = 146.7$). (b) Similarly, the separation of MCF-7 and RBCs is also achieved at 3.0 ml/h (see Movie S1 in the Supporting Information). The carrier medium was the denaturated 0.2 wt % PEO solution. The MCF-7 cells are marked by circles in the bright-field snapshot. (c) The normalized cell count plot is shown for the separation of MCF-7 cells and RBCs at 3.0 ml/h.

This size-based differential focusing phenomenon can be implemented in microfluidic devices for sheathless and label-free particle/cell separation. The stacked images in Figure 4 show an overlap between the streams of 15 μm and 5 μm particles for $AR = 1$, suggesting that high AR of cross-section is required for effective separation. In the microchannels with $AR = 2$ (Figure 5a), there was a much wider distance between two streams of 15 μm particles and 5 μm particles at flow rates ranging from 2.0 to 5.0 ml/h, resulting in complete separation. Figure 5 shows particle distributions at a wide range of flow rates. At the lowest flow rates ($Re = 0.28$ and 0.69 for $AR = 2$ and 4 , respectively), particles were focused at multiple equilibrium positions, which is similar to the case of pure elastic flow. We notice that the lowest Re at which the equilibrium positions around the channel corners vanish is higher for larger particles, which can be attributed to the stronger scaling of the inertial lift²⁴ with a than the elastic force²⁷ near the wall. As the Wi increases, elastic force becomes larger and particles focus more tightly at the equilibrium positions. At threshold flow rates ($Re = 5.6$

and 11.1 for $AR = 2$ and 4 , respectively), the shear gradient force starts to play an adverse role and make the focused 5 μm particles disperse. In the microchannels with $AR = 4$ (Figure 5b), 15 μm particles showed the similar focusing pattern as the case of $AR = 2$. However, 5 μm particles were not focused as tightly as in the case of $AR = 2$. The insufficient focusing of the 5 μm particles is due to the weaker viscoelastic force and enhanced inertia along the wide dimension in $AR = 4$ microchannels. The relative importance of elastic force and inertial force is characterized by the elasticity number El ($El = Wi/Re = 2\lambda\eta/\rho W^2$). The El for microchannels with $AR = 4$ is only a quarter of the El for $AR = 2$. Therefore, we conducted the particle/cell separation in $H = 50$ μm microchannels with $AR = 2$. At flow rates higher than 3.0 ml/h, the focusing of 5 μm particles slightly degraded due to increasing inertial lift. In addition, the spacing between two streams of 15 μm particles became narrower for flow rates exceeding 3.0 ml/h. Since large particles or cells can affect the focusing of their small neighbors by disturbing the surrounding flow field,^{63,64} an optimized flow rate of 3 ml/h was set for particle/cell separation.

The separation of 15 μm and 5 μm PS particles (Figure 6a) stemmed directly from the differential focusing of them (Figure 5a) in a microchannel with $H = 50$ μm and $AR = 2$ at the optimized flow rate of 3 ml/h. This sheathless approach can be easily applied to separate the binary mixture of MCF-7 cells and RBCs in a label-free manner. (Figure 6b and Movie S1 in the Supporting Information). Though having wider size distribution than the synthetic particles, RBCs were still tightly focused along the centerline as the 5 μm particles were, and MCF-7 cells, like the 15 μm particles, migrated along the streamlines that obviously deviated from the centerline, suggesting high-quality separation. Figure 6c shows the cell distributions at the outlet, indicating high separation efficiencies of 91.4% and 91.7% for MCF-7 cells and RBCs, respectively. Since the initial ratio of MCF-7 cells in the total cells is only 1.2%, even a small portion of RBCs mixed with MCF-7s at the outlet will reduce the purity significantly. The purity of MCF-7 cells is about 14.5%, but still with a high enrichment factor of 11.7. The separation degraded at higher flow rates due to the degradation of RBCs focusing and emergence of MCF-7 cells at the centerline. Still, the operating flow rate is one order magnitude higher than existing viscoelasticity-based separation.^{35,42,55} Though the present throughput (3×10^8 cells/h at 3 ml/h with 1% hematocrit) is an order of magnitude lower than that of typical inertial microfluidic devices ($\geq 10^9$ cells/h), good parallelizability of straight geometry can offset the relatively low throughput of a single channel. Several groups have demonstrated the feasibility of parallelization of tens³⁹ or even hundreds⁶⁵ of channels for the high throughput.

Separation of smaller particles and cells. By scaling down the channel size, we successfully demonstrate the complete separation of smaller particles (1 μm and 3 μm PS particles) and cells (*E. coli* bacteria and RBCs) in microchannels with $H = 10$ μm. Therefore, similar size-based separation was expected: the 1 μm particles/*E. coli* bacteria were focused along the centerline whereas the 3 μm particles/RBCs were focused near the side walls. The focusing of sub-micron particles with diameter around or less than 1 μm may degrade due to the diffusive effect of Brownian motion. The importance of Brownian diffusion can be characterized by

the Péclet number Pe , which is expressed as²⁷ $Pe = aV_e/D_0$ where V_e is the velocity of viscoelastic lateral migration, and

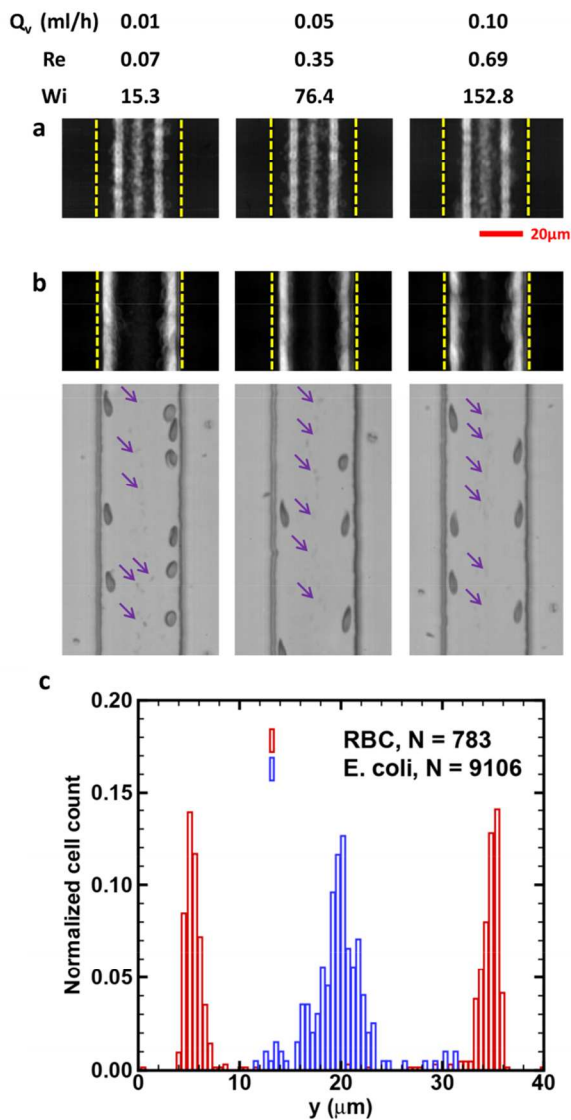


Figure 7. Complete separation of the binary mixtures of 3 μm and 1 μm particles (a) and RBCs and *E. coli* (b) can be achieved over a wide range of flow rates using the denaturated 0.2 wt % PEO solution, where the 3 μm particles/RBCs were focused along the both sides of the centerline whereas the 1 μm particles/*E. coli* were focused at the centerline. The *E. coli* were marked by arrows in the bright-field snapshots and can be seen more clearly in the Movie S2-4 in the Supporting Information. (c) The normalized cell count plot is shown for the separation of RBCs and *E. coli* bacteria at 0.1 ml/h.

D_0 is the Stokes-Einstein diffusivity of a particle.⁶⁶ For $a = 0.5 \mu\text{m}$ and $Q_v = 0.1 \text{ ml/h}$, the corresponding $Pe \sim O(10^4)$ indicates a negligible Brownian diffusion for the separation of *E. coli* bacteria and RBCs.

Concurring with expectation, high-quality separations of particles (Figure 7a) and cells (Figure 7b) were achieved in a microchannel with $H = 10 \mu\text{m}$ and $AR = 4$. Since it is difficult to identify the *E. coli* due to their small size, we took slightly out of focus bright-field images for easier identification (Figure 7b and the Movie 2-4 in the Supporting Information).

The distinctive size difference between *E. coli* and RBC resulted in a wide separation distance. Though the focusing of *E. coli* at the low flow rate of 0.01 ml/h was not as tight as that at the higher flow rates of 0.05 and 0.1 ml/h, the wide separation distance between *E. coli* and RBCs still made good separation achievable. Therefore, the separation remained high-quality over the flow rates of 0.01-0.1 ml/h. Figure 7c indicates a nearly complete separation between RBCs and *E. coli* bacteria at 0.1 ml/h. The separation efficiencies are estimated to be 94.1% and 99.9% for RBCs and *E. coli* bacteria, respectively. The purity of RBCs at the outlet is about 99.9% with an enrichment factor of 11.3. RBCs showed obvious deformation during the separation due to the exposure of high shear rate flow in confined space. As the exposure only persisted a very short period and, for instance, RBCs passed through the microchannel within 1 s at 0.1 ml/h in this study. It is expected that the separation only exerted negligible damage on RBCs.

CONCLUSIONS

In this study, we present sheathless, label-free, and inexpensive particle/cell separation in simple straight microchannels utilizing the size-based differential viscoelastic focusing. Complete separations of two binary cell mixtures of MCF-7 cells and RBCs, and *E. coli* bacteria and RBCs are realized by only tuning the channel size. The tight focusing of sub-micron *E. coli* bacteria suggests the potential of achieving high-quality focusing and separation even for nanoparticles. Using the denaturated 0.2 wt % PEO solution, the present device has reached optimized flow rates one order of magnitude higher than those of existing viscoelastic separation devices that use inexpensive synthetic polymers. We recommend further study on engineering rheological properties of carrier media for improving the separation performance of viscoelasticity-based microfluidic devices.

AUTHOR INFORMATION

Corresponding Author

*Phone: +86-10-82544298. Fax: +86-10-82543977. E-mail: guoqing.hu@imech.ac.cn.

Notes

The authors declare no competing financial interest.

ACKNOWLEDGMENT

We thank the Ministry of Science and Technology (2011CB707604, 2011CB707603) and the National Science Foundation of China (11272321, 11402274) for financial support. We sincerely thank Dr. Jiashu Sun from National Center for Nanoscience and Technology for providing MCF-7 cells and *Escherichia coli* bacteria to us.

Supporting Information Available

Movies for cell separation as noted in the text. This information is available free of charge via the Internet at <http://pubs.acs.org>.

REFERENCES

- (1) Krivacic, R. T.; Ladanyi, A.; Curry, D. N.; Hsieh, H. B.; Kuhn, P.; Bergsrud, D. E.; Kepros, J. F.; Barbera, T.; Ho, M.

- 1 Y.; Chen, L. B.; Lerner, R. A.; Bruce, R. H. *Proc. Natl. Acad.*
2 *Sci. U. S. A.* **2004**, *101*, 10501-10504.
- 3
4 (2) Toner, M.; Irimia, D. *Annu. Rev. Biomed. Eng.* **2005**, *7*, 77.
- 5
6 (3) Vincent, M. E.; Liu, W.; Haney, E. B.; Ismagilov, R. F.
7
8 *Chem. Soc. Rev.* **2010**, *39*, 974-984.
- 9
10 (4) Shannon, M. A.; Bohn, P. W.; Elimelech, M.; Georgiadis,
11
12 J. G.; Marinas, B. J.; Mayes, A. M. *Nature* **2008**, *452*,
13
14 301-310.
- 15
16 (5) Giddings, J. C. *Science* **1993**, *260*, 1456-1465.
- 17
18 (6) Xuan, X.; Zhu, J.; Church, C. *Microfluid. Nanofluid.* **2010**,
19
20 *9*, 1-16.
- 21
22 (7) Nagrath, S.; Sequist, L. V.; Maheswaran, S.; Bell, D. W.;
23
24 Irimia, D.; Ulkus, L.; Smith, M. R.; Kwak, E. L.; Digumarthy,
25
26 S.; Muzikansky, A.; Ryan, P.; Balis, U. J.; Tompkins, R. G.;
27
28 Haber, D. A.; Toner, M. *Nature* **2007**, *450*, 1235-1239.
- 29
30 (8) Lewpiriyawong, N.; Kandaswamy, K.; Yang, C.; Ivanov,
31
32 V.; Stocker, R. *Anal. Chem.* **2011**, *83*, 9579-9585.
- 33
34 (9) Yamada, M.; Nakashima, M.; Seki, M. *Anal. Chem.* **2004**,
35
36 *76*, 5465-5471.
- 37
38 (10) Gijjs, M. A. M.; Lacharme, F.; Lehmann, U. *Chem. Rev.*
39
40 **2009**, *110*, 1518-1563.
- 41
42 (11) Pamme, N. *Lab Chip* **2006**, *6*, 24-38.
- 43
44 (12) Wang, M. M.; Tu, E.; Raymond, D. E.; Yang, J. M.;
45
46 Zhang, H.; Hagen, N.; Dees, B.; Mercer, E. M.; Forster, A. H.;
47
48 Kariv, I.; Marchand, P. J.; Butler, W. F. *Nat. Biotechnol.* **2005**,
49
50 *23*, 83-87.
- 51
52 (13) Friend, J.; Yeo, L. Y. *Rev. Mod. Phys.* **2011**, *83*, 647-704.
- 53
54 (14) Laurell, T.; Petersson, F.; Nilsson, A. *Chem. Soc. Rev.*
55
56 **2007**, *36*, 492-506.
- 57
58 (15) MacDonald, M. P.; Spalding, G. C.; Dholakia, K. *Nature*
59
60 **2003**, *426*, 421-424.
- (16) Choi, S.; Park, J.-K. *Lab Chip* **2005**, *5*, 1161-1167.
- (17) Zhu, J.; Tzeng, T.-R.; Hu, G.; Xuan, X. *Microfluid. Nanofluid.* **2009**, *7*, 751-756.
- (18) Zeng, S. J.; Pan, X. Y.; Zhang, Q. Q.; Lin, B. C.; Qin, J. H. *Anal. Chem.* **2011**, *83*, 2083-2089.
- (19) Rodriguez, W. R.; Christodoulides, N.; Floriano, P. N.; Graham, S.; Mohanty, S.; Dixon, M.; Hsiang, M.; Peter, T.; Zavier, S.; Thior, I. *PLoS Med.* **2005**, *2*, e182.
- (20) Yamada, M.; Seki, M. *Lab Chip* **2005**, *5*, 1233-1239.
- (21) Zhang, X.-B.; Wu, Z.-Q.; Wang, K.; Zhu, J.; Xu, J.-J.; Xia, X.-H.; Chen, H.-Y. *Anal. Chem.* **2012**, *84*, 3780-3786.
- (22) Davis, J. A.; Inglis, D. W.; Morton, K. J.; Lawrence, D. A.; Huang, L. R.; Chou, S. Y.; Sturm, J. C.; Austin, R. H. *Proc. Natl. Acad. Sci. U. S. A.* **2006**, *103*, 14779-14784.
- (23) Balvin, M.; Sohn, E.; Iracki, T.; Drazer, G.; Frechette, J. *Phys. Rev. Lett.* **2009**, *103*, 078301.
- (24) Di Carlo, D.; Edd, J.; Humphry, K.; Stone, H.; Toner, M. *Phys. Rev. Lett.* **2009**, *102*.
- (25) Asmolov, E. S. *J. Fluid Mech.* **1999**, *381*, 63-87.
- (26) Ho, B. P.; Leal, L. G. *J. Fluid Mech.* **1976**, *76*, 783-799.
- (27) Leshansky, A. M.; Bransky, A.; Korin, N.; Dinnar, U. *Phys. Rev. Lett.* **2007**, *98*, 4.
- (28) Wu, Z.; Willing, B.; Bjerketorp, J.; Jansson, J. K.; Hjort, K. *Lab Chip* **2009**, *9*, 1193.
- (29) Mach, A. J.; Di Carlo, D. *Biotechnol. Bioeng.* **2010**, *107*, 302-311.
- (30) Hur, S. C.; Henderson-MacLennan, N. K.; McCabe, E. R. B.; Di Carlo, D. *Lab Chip* **2011**, *11*, 912-920.
- (31) Sun, J. S.; Li, M. M.; Liu, C.; Zhang, Y.; Liu, D. B.; Liu, W. W.; Hu, G. Q.; Jiang, X. Y. *Lab Chip* **2012**, *12*, 3952-3960.

- 1
2
3
4
5
6
7
8
9
10
11
12
13
14
15
16
17
18
19
20
21
22
23
24
25
26
27
28
29
30
31
32
33
34
35
36
37
38
39
40
41
42
43
44
45
46
47
48
49
50
51
52
53
54
55
56
57
58
59
60
- (32) Sun, J. S.; Liu, C.; Li, M. M.; Wang, J. D.; Xianyu, Y. L.; Hu, G. Q.; Jiang, X. Y. *Biomicrofluidics* **2013**, *7*.
- (33) Zhou, J.; Giridhar, P. V.; Kasper, S.; Papautsky, I. *Lab Chip* **2013**, *13*, 1919-1929.
- (34) Kuntaegowdanahalli, S. S.; Bhagat, A. A. S.; Kumar, G.; Papautsky, I. *Lab Chip* **2009**, *9*, 2973-2980.
- (35) Kang, K.; Lee, S. S.; Hyun, K.; Lee, S. J.; Kim, J. M. *Nat. Commun.* **2013**, *4*.
- (36) Lim, E. J.; Ober, T. J.; Edd, J. F.; Desai, S. P.; Neal, D.; Bong, K. W.; Doyle, P. S.; McKinley, G. H.; Toner, M. *Nat. Commun.* **2014**, *5*.
- (37) Liu, C.; Hu, G.; Jiang, X.; Sun, J. *Lab Chip* **2015**, *15*, 1168-1177.
- (38) Di Carlo, D.; Irimia, D.; Tompkins, R. G.; Toner, M. *Proc. Natl. Acad. Sci. U. S. A.* **2007**, *104*, 18892-18897.
- (39) Bruus, H. *Theoretical microfluidics*; Oxford University Press: Oxford, 2008.
- (40) Yang, S.; Kim, J. Y.; Lee, S. J.; Lee, S. S.; Kim, J. M. *Lab Chip* **2011**, *11*, 266-273.
- (41) Kim, J. Y.; Ahn, S. W.; Lee, S. S.; Kim, J. M. *Lab Chip* **2012**, *12*, 2807-2814.
- (42) Nam, J.; Lim, H.; Kim, D.; Jung, H.; Shin, S. *Lab Chip* **2012**, *12*, 1347-1354.
- (43) Morozov, A. N.; van Saarloos, W. *Phys. Rep.* **2007**, *447*, 112-143.
- (44) Crumeyrolle, O.; Mutabazi, I.; Grisel, M. *Phys. Fluids* **2002**, *14*, 1681-1688.
- (45) Stone, P. A.; Waleffe, F.; Graham, M. D. *Phys. Rev. Lett.* **2002**, *89*, 208301.
- (46) Karimi, A.; Yazdi, S.; Ardekani, A. M. *Biomicrofluidics* **2013**, *7*, 23.
- (47) D'Avino, G.; Romeo, G.; Villone, M. M.; Greco, F.; Netti, P. A.; Maffettone, P. L. *Lab Chip* **2012**, *12*, 1638-1645.
- (48) Romeo, G.; D'Avino, G.; Greco, F.; Netti, P. A.; Maffettone, P. L. *Lab Chip* **2013**, *13*, 2802-2807.
- (49) Tirtaatmadja, V.; McKinley, G. H.; Cooper-White, J. J. *Phys. Fluids* **2006**, *18*, 043101.
- (50) Doi, M.; Edwards, S. F. *The theory of polymer dynamics*; Clarendon Press Oxford: Oxford, 1986.
- (51) Rodd, L. E.; Scott, T. P.; Boger, D. V.; Cooper-White, J. J.; McKinley, G. H. *J. Non-Newton. Fluid Mech.* **2005**, *129*, 1-22.
- (52) Gauthier, F.; Goldsmith, H. L.; Mason, S. G. *J. Rheol.* **1971**, *15*, 297-330.
- (53) Huang, P. Y.; Joseph, D. D. *J. Non-Newton. Fluid Mech.* **2000**, *90*, 159-185.
- (54) Huang, P. Y.; Feng, J.; Hu, H. H.; Joseph, D. D. *J. Fluid Mech.* **1997**, *343*, 73-94.
- (55) Lee, D. J.; Brenner, H.; Youn, J. R.; Song, Y. S. *Sci. Rep.* **2013**, *3*.
- (56) Dhahir, S. A.; Walters, K. *J. Rheol.* **1989**, *33*, 781-804.
- (57) Cha, S.; Kang, K.; You, J.; Im, S.; Kim, Y.; Kim, J. *Rheol. Acta* **2014**, 1-7.
- (58) Carew, E. O. A.; Townsend, P. *Rheol. Acta* **1991**, *30*, 58-64.
- (59) Del Giudice, F.; Romeo, G.; D'Avino, G.; Greco, F.; Netti, P. A.; Maffettone, P. L. *Lab Chip* **2013**, *13*, 4263-4271.
- (60) Villone, M. M.; D'Avino, G.; Hulsen, M. A.; Greco, F.; Maffettone, P. L. *J. Non-Newton. Fluid Mech.* **2013**, *195*, 1-8.
- (61) Yang, S.; Lee, S. S.; Ahn, S. W.; Kang, K.; Shim, W.; Lee, G.; Hyun, K.; Kim, J. M. *Soft Matter* **2012**, *8*, 5011-5019.
- (62) Zhou, J.; Papautsky, I. *Lab Chip* **2013**, *13*, 1121-1132.

1 (63) Amini, H.; Sollier, E.; Weaver, W. M.; Di Carlo, D. *Proc.*

2 *Natl. Acad. Sci. U. S. A.* **2012**, *109*, 11593-11598.

3
4 (64) Bhagat, A. A. S.; Hou, H. W.; Li, L. D.; Lim, C. T.; Han,

5
6 *J. Lab Chip* **2011**, *11*, 1870-1878.

7
8 (65) Hur, S. C.; Tse, H. T. K.; Di Carlo, D. *Lab Chip* **2010**, *10*,

9
10 274-280.

11 (66) Welty, J. R.; Wicks, C. E.; Rorrer, G.; Wilson, R. E.

12 *Fundamentals of momentum, heat, and mass transfer*; John

13
14
15
16 Wiley & Sons: Hoboken, 2009.

17
18
19
20
21
22
23
24
25
26
27
28
29
30
31
32
33
34
35
36
37
38
39
40
41
42
43
44
45
46
47
48
49
50
51
52
53
54
55
56
57
58
59
60

1
2
3
4
5
6
7
8
9
10
11
12
13
14
15
16
17
18
19
20
21
22
23
24
25
26
27
28
29
30
31
32
33
34
35
36
37
38
39
40
41
42
43
44
45
46
47
48
49
50
51
52
53
54
55
56
57
58
59
60

For TOC only

